Template for a 2021 ASABE Annual Meeting Paper

Use this template for correct online indexing and searches.

All meeting papers will be included in the ASABE Online Technical Library at https://elibrary.asabe.org/toc.asp.

Deadline - For your paper to be posted online ***before*** the meeting, upload your completed paper by **May 3, 2021**, at https://na.eventscloud.com/eSites/580019/Homepage

Papers uploaded ***after*** May 3, 2021, will be posted after the meeting.

The ITSC Paper Awards deadline is April 20, 2021.

The name of your Microsoft Word file should match your paper number.
Example file name: 2199999.docx

You must enter your paper number in THREE locations below.

Have questions? Click on the FAQ.

- Please follow these instructions. Processing time is delayed when these instructions are not followed.
- The tables below are necessary for online indexing of author names. They will not be printed with your paper.
- The title, abstract, keywords, etc. of your paper ***must*** have certain Word styles for online searches.
- There are instructions below about fonts, styles, and references. Use website links for help. Use Times New Roman font for text except inside figures. Within figures, use a sans serif font, such as Arial, for clarity; however, the caption under the figure should be Times New Roman. For citations in the text, use the name, date system. For the references section at the end of the paper, use *APA 6th* style. These changes make this paper like our journal format. You may want to publish this paper in our journals. See https://www.asabe.org/JournalAuthors for more.
  Revised 12/15/2020.

See the ASABE website for more information for authors and about ASABE templates.

Author 1 (one author only)

First Name (or initial)	Middle Name (or initial)	Surname	Suffix (Jr., III, etc.)	Role (ASABE member, etc.)	Email	Contact author? yes or no
Kushal		KC		Member	kc.7@osu.edu	Yes

Affiliation for Author 1

Organization	Address	Country	Phone for contact author
The Ohio State University	590 Woody Hayes Drive, Columbus OH 43210	USA	614-4401-059

Author 2 (one author only)

First Name (or initial)	Middle Name (or initial)	Surname	Suffix (Jr., III, etc.)	Role (ASABE member, etc.)	Email	Contact author? yes or no
Sami		Khanal			khanal.3@osu.edu	yes

Affiliation for Author 2

Organization	Address	Country	Phone for contact author
The Ohio State University	590 Woody Hayes Drive, Columbus OH 43210	USA	313-595-1001

Paper number and page range

Paper number on the line below ***[Click here to enter paper number]***
Pages 1-18

2950 Niles Road, St. Joseph, MI 49085-9659, USA
269.429.0300 fax 269.429.3852 hq@asabe.org www.asabe.org

An ASABE Meeting Presentation
DOI: https://doi.org/10.13031/aim.2100871
Paper Number: 2100871

Assessment of the Spatial and Temporal Patterns of Cover Cropping practices in the Western Lake Erie Basin

[1]Kushal KC, and [1]Sami Khanal*
Department of Food, Agricultural and Biological Engineering, The Ohio State University, Columbus OH 43210, USA

ABSTRACT. *Cover cropping is one of the conservation practices that could help alleviate soil health problems and reduce nutrient losses to water resources. Although there exist substantial scientific research and evidence about cover crops and their impacts on soil and water quality, they are based mainly on controlled field experimental trials. Currently, there is a limited understanding of spatial and temporal trend in cover cropping practices and their impacts at a landscape scale. Thus, the objective of this study is to develop a spatial and temporal inventory of winter cover cropping practices in a Western Lake Erie Basin, Maumee River watershed using satellite remote sensing. We created a long-term seasonal composites of satellite images (Landsat 5, 7 and 8) from 2008 to 2019. Then image-based covariates for 255 fields were used to develop a cover crop classification model based on the Random Forest algorithm. The image composites were then classified into four categories- (1) winter hardy, (2) winter kill, (3) spring emergent, and (4) not covered. The overall accuracy of the classification was 0.78, with kappa coefficient of 0.57 Our results show that more than 50% of the corn-soybean area in the watershed was not covered with winter vegetation during 2008-2019 period. The total cover cropping area however has increased by about 40% in 2019/20 season compared to 2008/09 season. Based on our analysis of trend in winter weather, cover crops tend to perform well with higher accumulated Growing Degree Days and fall precipitation.*

Keywords. *Cover crop, Remote Sensing, Machine learning, Western Lake Erie basin, Random Forest*

1. Introduction

There is a growing consensus that common agricultural practices are leading to a widespread soil degradation, poor soil health and water quality problems. Cover cropping has been recommended as one of the effective best management practices (BMPs) for addressing these problems while improving crop productivity and farm profitability [1,2]. Cover crops help improve soil and water quality by reducing soil compaction, fixing nitrogen in soil, enhancing soil organic matter, and reducing nutrient losses through soil erosion and surface runoffs [3–6] Additionally, cover cropping has been found to provide several other ecosystem services including reduction of greenhouse gas emissions, control of weeds and enhancement of biodiversity [7–9].

Cover crops can be in various forms including grass-legume, brassica, small grain, or their mixture that are grown during a fallow period between two growing seasons. Although they are not new to US agriculture system and have several environmental benefits, they are less adopted due to agronomic, economic and operational challenges [10]. As such, there are several state and federal funding programs such as NRCS Environmental Quality Incentives Payment (EQIP) and Conservation Stewardship Program (CSP) that have promoted the adoption of BMPs including cover crops to promote soil health and mitigate widespread water quality problems. According to 2017 Census of Agriculture, national cover crop acreage increased by 50 percent from 2012 to 2017, with several states including Ohio doubled their acreage. Based on the survey, the total cover crop area of Ohio in 2017 was 7% of the total cropland in the state. Although helpful, surveys provide an incomplete representation of the overall practices on the ground and thus do not provide information about the spatial and temporal coverage of cover crops at a landscape scale. Further, surveys are expensive to conduct at a larger geographic scale and are often biased. Similarly, most of our current understanding of cover crop are based on field-scale trials at limited fields, and thus findings may not be transferrable to other cover crop growing sites.

Remote sensing, particularly satellite-based imagery, offers a promising approach to cost-effectively and timely detect and monitor vegetation health at a landscape scale. This capability has recently been bolstered by a wide availability of a large volume of data from frequently revisiting medium-resolution satellites such as Landsat (30 m) and Sentinel (10 m) at free of cost. Green and healthy vegetations have higher reflectance in near-infrared (NIR) region than other spectral region, and thus, prior studies have leveraged satellite imagery in the visible and NIR region (VIS-NIR) to understand and classify difference in crop health [11–13] . Data including 30-meter National Land Use Land Cover and annual cropland data layer are some of the key applications of satellite-based remote sensing [2,14–18], which were derived from Landsat satellite and other digital data [19]. In contrast to broad land use land cover classes, cropland areas are dynamic and change over both spatial and temporal scales because of several factors including growing season, management practices and environmental conditions. In such, remote sensing data have been proven valuable for large area crop type as well as crop related land use classification because of its large and repeated coverage suitable for capturing different growing patterns of different crops [18,20].

There are a few prior studies that have used satellite-based remote sensing data to classify and monitor winter cover crops at a landscape scale on limited geographic regions [21–26]. For instance, Hively et al (2015) assessed cover crop areas in Chesapeake Bay watershed in southeastern Pennsylvania using satellite data and reported increase in cover crop adoption between 2010 and 2013 [26]. It was based on one-time best Landsat and SPOT imagery during late winter. In another study, Landsat-7 and Landsat-8 satellite images from fall and spring were used in combination with ground collected NDVI threshold to identify cover cropped fields [21]. Both these studies applied the calibrated threshold on the single one-time satellite images and also reported missing data due to cloud cover or scan line error of Landsat-7. This also limited the study to only specific location where the data were available consistently. Seifert et al (2018) mapped cover crop areas from 2008 to 2016 over the eight Midwestern states combining multiple Landsat satellite images (Landsat 5, 7, and 8) from each cover crop growing season (i.e., October - April) as a single seasonal composite [24]. This allowed them to get rid of incomplete coverage or gaps in the images and derive a consistent coverage for whole study area unlike previous studies. Although helpful, single composite of satellite data for each growing season smooths out temporal variability in cover crop phenology, and thus it becomes difficult to quantify their characteristics (e.g., winter kill, winter hardy, spring emergence, no cover) other than absence or presence on the fields. Unlike Seifert et al (2018), Hagen et al (2020) (estimated timing and intensity of greenness of cover crops based on a time series of the normalized difference vegetation index (NDVI) from November through July of each crop year and compared to threshold sets at the HUC8 scale to determine cover crop status in the midwestern United States from 2005 to 2018 [22]. It seemed like the HUC8 threshold set were selected based on integration of ground-truth and satellite imagery beforehand. Although the study did not explicitly mention on how they use all the images (individually or developing composites), it showed that we can utilize the variability in the growing pattern to identify different types of winter covers on the croplands. This can be still achievable with the use of compositing technique, increasing the number of seasonal composites can enable us to capture sub-seasonal growth patterns. This also helps avoid the need for several satellite observations for all pixel's location to one or more predetermined periodic representations [27]. Additionally, the recent developments in cloud processing platforms such as Google Earth Engine (GEE) has provided the scientific community a tool to access a vast pool of satellite imagery as well as process images using state-of-the-art data

analytics while addressing the computational time and efficiencies [28]. As such, in recent years, GEE has emerged as a valuable tool for conducting regional- [29–31] to global-scale earth observation-based research studies [32,33].

The objectives of this study are to 1) quantify the spatial and temporal trends of winter covers in the Maumee river watershed, one of the largest watersheds in the Great Lakes basin, between 2008 and 2019 by integrating historical satellite time-series data with ground-truth observations in the GEE platform, and 2) examine the spatial and temporal patterns of cover crop growth in relation to weather, mainly precipitation and temperature, at a landscape scale.

2. Methods

2.1 Study Area

Although Western Lake Erie basin has been continuously highlighted as one of the most impaired basins, there are not many studies studying the trend of conservation practices in the region. The study was conducted in the Maumee River watershed in the northwest Ohio, where agriculture is the predominant land use (Figure 1). About 80% of this watershed is in corn and soybean production, and studies have related intensive agricultural practices associated with corn and soybean production in this region as the primary drivers of more than 85% of phosphorous loads to the Maumee River, which eventually drains to the Lake Erie[34,35]. This has been the primary reason for increase in harmful algal blooms, causing undesirable impacts on fish habitat, decreased recreational uses of waterways, problems in drinking water supplies, and increased costs of water treatment and managing freshwaters. Since cover crops can provide a ground cover that reduces runoffs and increases infiltration of water into the soil, there is increasing interest on cover crops as one of the conservation practices to mitigate these problems in recent years [5]. However, surveys have suggested a slow adoption of cover crops by farmers in this watershed, only 16.8%, 17.6%, and 11.9% of farmers adopted cover crops on their low, medium and highly productive fields respectively (2014 survey) [36] .

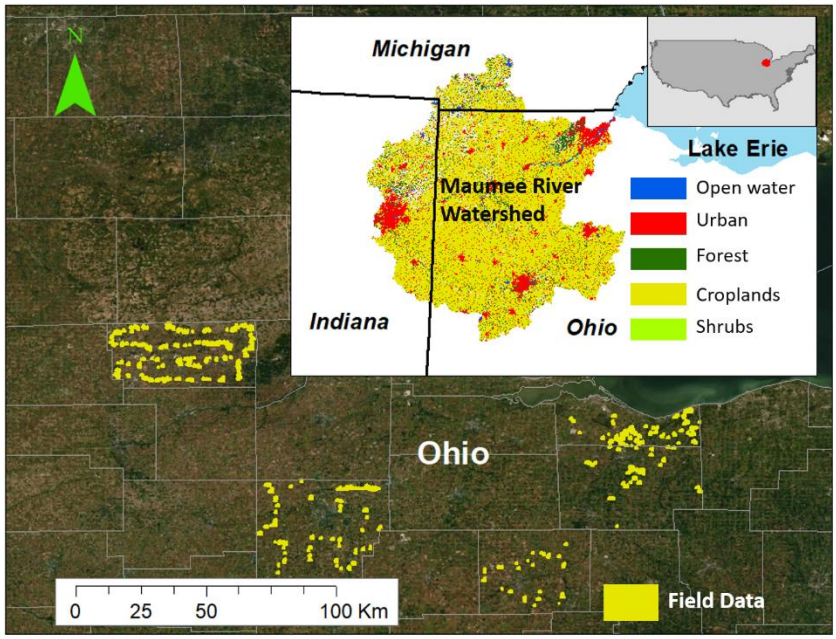

Figure 1: Maumee River watershed spreading over Ohio, Indiana, and Michigan in the Midwest United States. A large portion of watershed is used for agriculture mainly corn and soybean. Field data used in the study are highlighted in yellow.

2.2 Data

Satellite Data Acquisition and Processing

In the study, images covering northern and north-west part of Ohio collected by Landsat satellite 5, 7 and 8 between 2008 to 2020 were used. The selection of images from various Landsat missions was based on their lifespans and availability of historic time-series satellite data (Table 1). The satellite images with cloud cover less than 50% were collected for each growing season of cover crop (October – April of following year) for the entire study period.

To facilitate easier and faster preprocessing and analyses of these satellite data, Google Earth Engine (GEE), a cloud-based platform developed and made publicly available by Google [28], was used. Specifically, we used JavaScript based Earth Engine Code Editor to process Level-2 surface reflectance (SR) products from Landsat, which were corrected for atmospheric attenuation and disturbances on each individual scene. SR data products from Landsat 5 and 7 were derived using the Landsat Ecosystem Disturbance Adaptive Processing System (LEDAPS) developed by National Aeronautics and Space Administration (NASA) and the University of Maryland [37]. Meanwhile SR data products from Landsat 8 were generated using Land Surface Reflectance Code (LaSRC) developed by NASA and later updated by USGS Earth Resources Observation and Science (EROS) Center [38]. We used Quality Assessment (QA) band generated using CFMask algorithm [39] to all the Landsat scenes to get rid of unwanted contamination of image pixels due to cloud, cloud shadow, and snow and provide accurate representation of vegetation health.

Table 1: Landsat satellites missions considered for the study

Dataset	Data Products	Spatial resolution	Temporal resolution	Launch	Data Availability
Landsat 8 OLI	Level-2 SR	30 m	16 days	2013	2013-Present
Landsat 7 ETM+	Level-2 SR	30 m	16 days	1999	2000-Present
Landsat 5 TM	Level-2 SR	30 m	16 days	1984	1984-2012

Despite the fact that the images are collected by same satellite system, there exist slight differences in the spectral signatures of same object when analyzed using data based on three Landsat missions (Thematic Mapper (TM), Enhanced Thematic Mapper Plus (ETM+), and Operational Land Imager (OLI)). For both soil surfaces and vegetations, Roy et al (2016) observed higher Normalized Difference Vegetation Index (NDVI) derived from ETM+ images compared to those derived from OLI images [40]. The study developed spectral transformation functions between OLI and TM/ETM+ data by fitting an ordinary least squares (OLS) regression with $r^2 > 0.7$ for reflectance and > 0.9 for NDVI. The slopes and intercepts of this equation corresponding to each individual band are shown in the Equation 1.

$$Intercept = [0.0003, 0.0088, 0.0061, 0.0412, 0.0254, 0.0172]\ for\ (Blue, Green, Red, NIR, SWIR1, SWIR2) Slopes = [0.8474, 0.8483, 0.9047, 0.8462, 0.8937, 0.9071]\ for\ (Blue, Green, Red, NIR, SWIR1, SWIR2)$$

$$Slopes = [0.8474, 0.8483, 0.9047, 0.8462, 0.8937, 0.9071]\ for\ (Blue, Green, Red, NIR, SWIR1, SWIR2)$$

Equation 1: Band specific transformation coefficients in terms of slope and intercept of the regression between ETM+ and OLI spectral space (Roy et al., 2016)

To ensure these differences are resolved for long-term time series analyses, TM and ETM+ based images were transformed into OLI spectral space using the slopes and intercepts value in equation 1. This process is also called harmonization, which has been found to be useful in eliminating several issues that are part of satellite data such as missing data due to SLC off, cloud cover, and shadow removal [15,41].

Since our study region is big, it was difficult to find a series of individual image scene covering the same geographic extent across multiple dates during the growing season. To capture crop phenology by analyzing images collected at multiple dates, we implemented a concept of seasonal composites by considering mean or median of satellite images collected during a given cover crop growing season [31,42–44]. Typically, the choice on the number of seasonal composites detects how closely the variabilities in a growing season needs to be assessed.

To determine the number of seasonal composites suitable for analyzing and monitoring the growth and extent of cover crops at a landscape scale, we plotted historical normal temperature profile (minimum, mean, and maximum) which was computed taking average of data from 8 locations across the Maumee River watershed. In the study region, we found that the month of December marks the start of cold winter (i.e., extreme weather condition unsuitable for cover crops growth) (Figure 2). Therefore, we divided the cover crop growing season into two time periods: Fall (before the onset of winter; most of the growth occurs in the month of October and November) and Spring (both winter and spring months; the significant growth occurring in the months of March and April) [45]. It was assumed that some cover crop species like cereal rye are cold tolerant in comparison to other species and can make all the way from fall to spring, while others are not tolerant and thus get terminated before winter or naturally die. Some species that are not able to grow properly during fall months show some growth during spring.

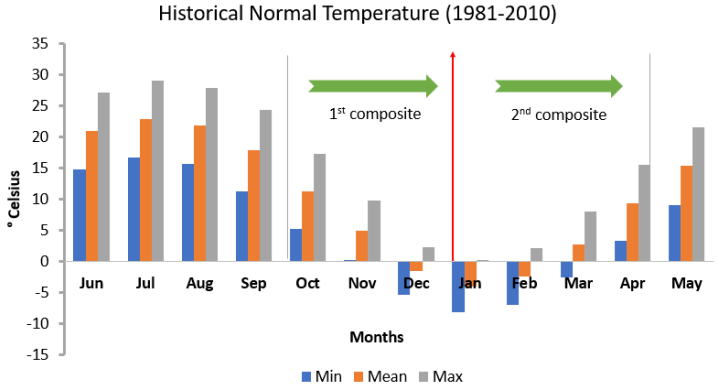

Figure 2: Historical mean weather plotted based on average of weather data from 8 locations in the Western Lake Ere basin. The data was collected from PRISM Climate Group [46]which provides 1895 to the present climate information.

We also used a harmonic analysis (also known as Fourier transformation) on Landsat 8 TOA NDVI computed by averaging all the pixels inside the cover crop fields (Figure 3), to analyze and characterize the underlying seasonal phenology of cover crops in the study region [47]. Fourier series or Fourier transform models any time series data as a combination of sine and cosine curves parametrized by amplitude/phase as well as distribution of frequency (Ryan, 1971; Davis et al., 1986). While amplitude is computed as half the height of a wave, phase is determined by how off the peak of the curve from the origin (0 to 2π). Addition of successive harmonics in the transformation brings the curve closer to the original curve. Similar to prior works [48,49], we found that cover crops follow bimodal structure and the amplitude of second order harmonic was dominant for about 73% of the total fields (Figure 3).

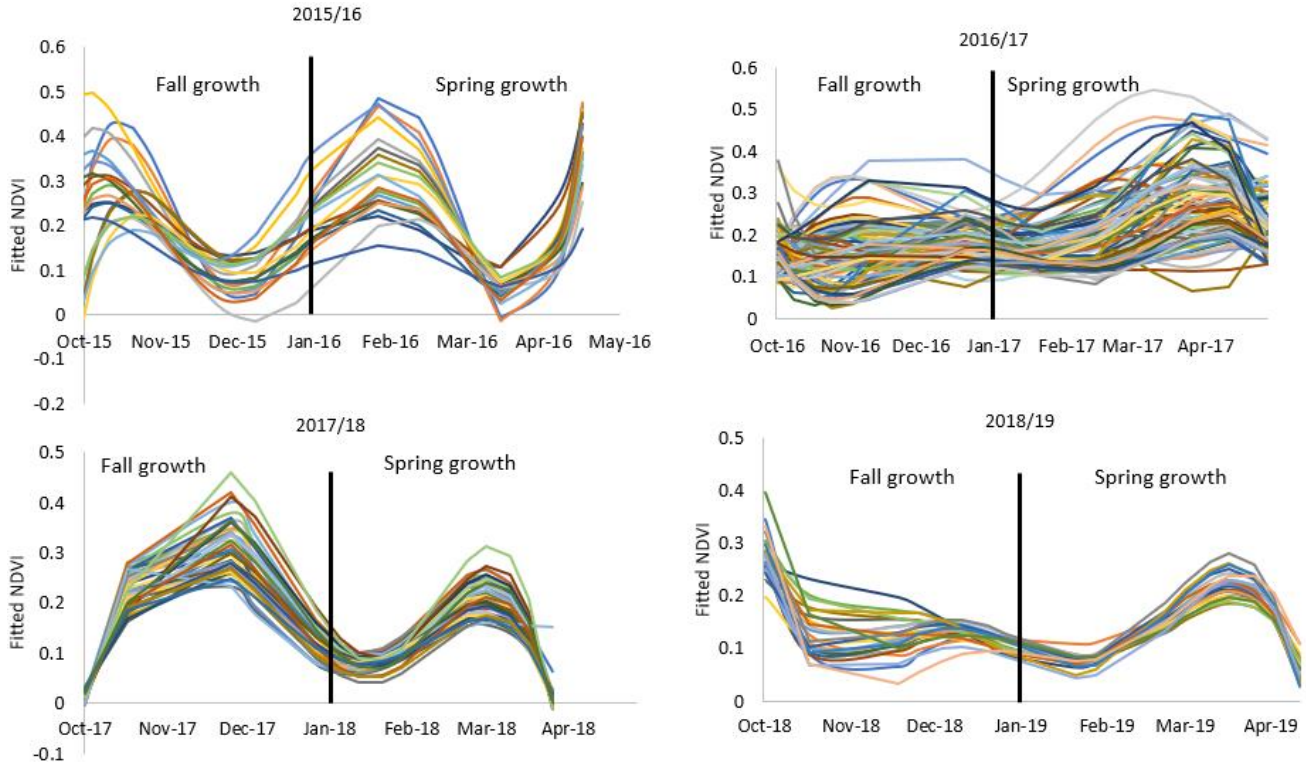

Figure 3: Second order harmonic. These curves are based on only the initial 255 fields from Erie and Huron counties. The NDVI value for each date is the average of all pixels within the field boundary.

To capture these seasonal dynamics, two seasonal composites of satellites data were prepared. First composite for October to December and second composite for January to April (Figure 3). While preparing these composites, the median of pixel values for a corresponding period were considered. Since the focus of the study was to assess cover crop presence on fields in corn and soybean rotation during summer, these seasonal composites were masked using 30 m resolution annual Cropland Data Layer (CDL) created by National Agricultural Statistics Service (NASS) [50] and is available in the GEE platform.

Issue of incomplete coverage and missing data

Despite the temporal aggregation of satellite images, some data gaps were observed in seasonal composites, particularly, 2012/2013 for the first composite, and 2009/10, 2012/2013, 2014/2015, 2017/2018 for the second composite. This was mainly driven by 16 days temporal resolution of Landsat satellite data in combination with frequent cloud cover and snow cover. To address this concern, we used fused and smoothened images derived using the Highly Scalable Temporal Adaptive Reflectance Fusion Model (HISTARFM) algorithm for the areas with such data gap. This algorithm uses 16-day Landsat and daily MODIS to produce monthly images at Landsat resolution i.e., 30 m [51]. Despite some differences in the range of wavelength covered by this product in comparison to Landsat 8 OLI, the study [51] found a good correlation (0.85-0.92) between the original Landsat band reflectance and the predicted HISTARFM band reflectance.

In addition to individual median bands, we created and added several commonly and widely used vegetation indices (VIs), such as NDVI [13,24,44,49,52,53], Difference Vegetation Index (DVI), Normalized Green Red Difference Index (NGRDI) [54] and Ratio Vegetation Index (RVI) [55] on the composites. Similarly, we created and added minimum, and maximum composites of NDVI as they have been proven as useful as median composite in mapping of crops [14,24]. For this, we used pixel-based reducer function in GEE. As such, each composite consisted of 12 bands (Table 2), with each band representing a feature of image pixels on a particular season. Each season thus has two composites: composite 1 (October to December) and composite 2 (January to April) (Figure 4).

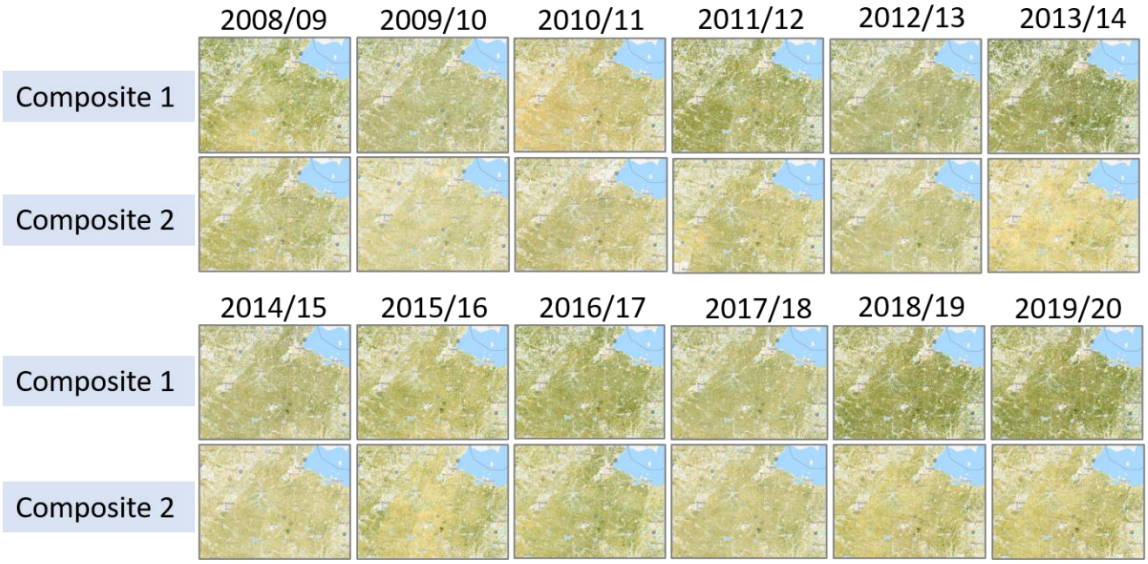

Figure 4: Landsat satellite image composites after gap filling and are displayed using natural color bands. For each winter season, two composites are created. Composite 1 represents fall growth (from October to December) and 2 represents spring growth (from January to April).

Table 2: Bands and indices that are included in each seasonal composite. Each of these components are treated as features of the pixels.

Composite Band	Description	Composite Band	Description
Blue_median	Median of blue band	DVI_median	Median of DVI
Green_median	Median of Green band	NDVI_median	Median of NDVI
NIR_median	Median of NIR band	NDVI_max	Maximum of NDVI
Red_median	Median of Red band	NDVI_min	Minimum of NDVI
SWIR1_median	Median of SWIR1 band	NGRDI_median	Median of NGRDI
SWIR2_median	Median of SWIR2 band	RVI_median	Median of RVI

Note: NIR – Near Infrared, SWIR – Shortwave Infrared, DVI – Difference Vegetation Index, NDVI – Normalized Difference Vegetation Index, NGRDI – Normalized Green Red Difference Index, RVI – Ratio Vegetation Index

Field data

A total of 657 cover crop fields across five counties in Northern Ohio (Figure 1) were used for analyses. Of these fields, information about 255 fields were gathered between 2015 to 2018 by Cover Crop Aggregation Program from Erie and Huron counties. Additional 402 records were based off tillage transect surveys from 2015 to 2019 in Fulton, Hancock, and Crawford counties in Ohio. These field points were digitized to their corresponding field boundaries. The field boundaries were then buffered inward by 30 m (equals to the Landsat resolution) to get rid of any potential mixed pixels during field data extraction [24]. For each winter season, there were different numbers of cover crop fields (Table 3). Although these fields were observed to have ground covers during the time of survey, it does not mean the fields were covered throughout the season, which can be influenced by weather, field conditions, and management practices.

To analyze the growth pattern or phenology of cover crops, we first applied a threshold of 0.3 on the average NDVI of cover crop fields. Based on this threshold, we filtered and labelled the fields into four categories: winter hardy (significant growth in fall and spring), winter kill (significant growth only in fall), spring emergent (significant growth in spring), and not covered (no significant growth in both periods). The NDVI value greater than 0.3 corresponds to the low to high vegetation cover of winter crops [25,26].

Table 3: NDVI criteria to characterize winter cover crops growth. It was computed by averaging all the pixels inside a field boundary during fall and spring season.

Criteria	Class	Number of fields
Fall NDVI and Spring NDVI >= 0.3	Winter-hardy	338
Fall NDVI > =0.3and Spring NDVI < 0.3	Winter kill	134
Fall NDVI < 0.3 and Spring NDVI > =0.3	Spring emergent	24
Fall NDVI and Spring NDVI < 0.3	Not covered	132

Note: 29 fields had missing pixels because of masking with annual CDL. These fields were not on either corn or soybean in those years. Field numbers by cover crop season: 135(2015/16), 185(2016/17), 84(2017/18), 87(2018/19), 166(2019/20)

Fields were then randomly split into training (60%) and validation (40%) groups. This was done to get rid of spatial autocorrelation that could arise from splitting the pixels from the same field into training as well as validation data [24,42].. For each field in training and validation group, we sampled the corresponding year's image composites. This resulted in 38,632 pixels for training and 30,124 pixels for validation.

2.3 Cover crop classification

While several algorithms are available to detect and classify crops and vegetation on satellite images, one of the critical questions is performance and accuracy. Among different machine learning algorithms, Random Forest (RF) classifier has become one of the most popular and widely applied in remote sensing community in recent years [17,56–58]. RF has been found to consistently outperform other classification algorithms particularly for applications related to crop classifications [59–61]. Similarly, it is robust against noise and overfitting, easier to train, and can handle high data dimensionality [62,63]. It is an ensemble of individual uncorrelated decision trees, created from the random bootstrap samples that use randomly selected subset of features [64]. The final output of this algorithm is calculated by aggregating outputs from all the decision trees, with a majority of voting used for classification and averaging of outputs for regression. It implements the bagging technique to randomly sample the data with replacement, and thus, it is expected to perform well even with small training dataset [65]. The only parameter we care most in common practice is the number of decision trees, increasing this number improves overall accuracy of the classification [64]. Other parameters that can be changed are the size of bootstrap sample, and number of feature subset chosen at each node split. Although RF is not sensitive to number of features at each node in decision trees, a common practice for subset size is square root of the number of features in the data [63,66]

We performed the sampling of field data within the GEE platform and combined them separately in python programming platform. The sampled data were aggregated together, we ran few trials in python to set the parameters up because of flexibility in python. We then uploaded the aggregates of sampled data back to the GEE platform. The randomForest classifier in GEE requires six arguments: numberOfTrees (default: 1), variablesPerSplit (default: square root of number of variables), minLeafPopulation (default: 1), bagFraction (default: 0.5), outOfBagMode (default: false), and seed (default: 0). We set the tree numbers to 500 based on commonly used practice [63] and other variables to default.

The classifier was trained using the sampled data and the accuracy of trained classifier was tested using an independent set of validation data. We evaluated the accuracy of classification results using the confusion matrix, which shows the distribution of classification results for the independent validation data sets against their true classes. We use metrics such as overall accuracy, Kappa coefficient, producer accuracy (PA) and user accuracy (UA). While an overall accuracy provides an average of accuracy for all classes considered, PA and UA provide the distribution of classification errors among the four classes. PA explains how many pixels for a particular class is classified correctly with respect to the actual number of pixels labeled on that class. UA explains how many pixels on the classified map truly represent the actual classes. After testing of the trained RS classifier, it was then used for classifying the seasonal composites from 2008/09 through to 2019/20 winter season into the four classes: winter hardy, winter kill, spring emergent, and not covered. Although the spatial extent of the images and classification was for most of the northern parts of Ohio including the Maumee River watershed due to the availability of training data from counties across the Western Lake Erie basin, we have shown findings only for the Maumee watershed in this work. Similarly, the findings have been shown only for fields that have been in corn and soybean rotation.

2.4 Weather variability and cover crop areas

We computed the GDD in GEE using the PRISM Daily Spatial Climate Dataset with spatial resolution of 2.5 arc minutes which is equivalent to 4 km. Daily mean temperature was used setting up the base temperature at 5 °C. Meanwhile the calculation was performed for the two periods of a season: fall (start of October to end of December) and spring (start of January to end of April). GDD for each day was calculated as

GDD = Tmean – Tbase,
Where Tmean is daily average temperature calculated as (Tmin + Tmax)/2
Tbase is the base temperature. If the average temperature was lower than the base temperature, then GDD was set to zero.

The accumaulated GDD for the two seasons (fall and spring) were computed by taking the sum of all the GDD during the period. For example, to obtain accumulated GDD for Fall of 2019, we added all the GDD value during October – December period. Similarly, we also extracted total accumulated precipitation during the months of October and November using the same PRISM Daily Climate dataset. It was done by taking the sum of all the pixels of daily precipitation raster data during that period. We repeated the process for every cover crop season from 2008/09 until 2019/20 and compared the trend with the annual cover crop areas to understand if there is any relationship between weather and abundance of cover crops at a landscape scale.

3. Results

3.1 Accuracy assessment

The RF classification resulted in overall accuracy (OA) of 74% and Kappa coefficient of 0.63 (Table 4). While winter hardy (75.39% and 82.56%) and no cover (80.84% and 80.33%) classes had higher PA and UA, winter kill class had moderate values of PA and UA (66.79% and 64.47%) and the spring emergent class had the lowest PA and UA (57.42% and 40.07%). Most of the misclassification of this spring emergent class has occurred to the no cover and winter hardy class as observed on the confusion matrix.

Table 4: Accuracy of classification results presented via confusion matrix.

		Predicted					
	Class	**Winter hardy**	**Winter kill**	**Spring emergent**	**No cover**	**Total**	**PA**
Ground Truth	**Winter hardy**	8,168	895	813	958	10,834	75.39%
	Winter kill	1,144	4,300	7	987	6,438	66.79%
	Spring emergent	279	37	843	309	1,468	57.42%
	No cover	302	1,438	441	9,203	11,384	80.84%
	Total	9,893	6,670	2,104	11,457	30,124	
	UA	82.56%	64.47%	40.07%	80.33%		
	Overall Accuracy 74.7%				**Kappa 0.63**		

Note: The rows indicate the actual values of pixels whereas the columns represent predicted values. The diagonal cells highlighted by color represent number of correctly classified pixels.

3.2 Cover crop areas: pixel-level estimates and temporal patterns

The pixel level classification of satellite image composites showed that a small area of the watershed was covered for most of the time between 2008-2019 (Figure 5). The area of cover crops ranged between 10% and 34%, with 2011/12 and 2019/20 having the highest percentage of watershed in cover crops and 2010/11, 2012/13, and 2014/15 with least percentage.

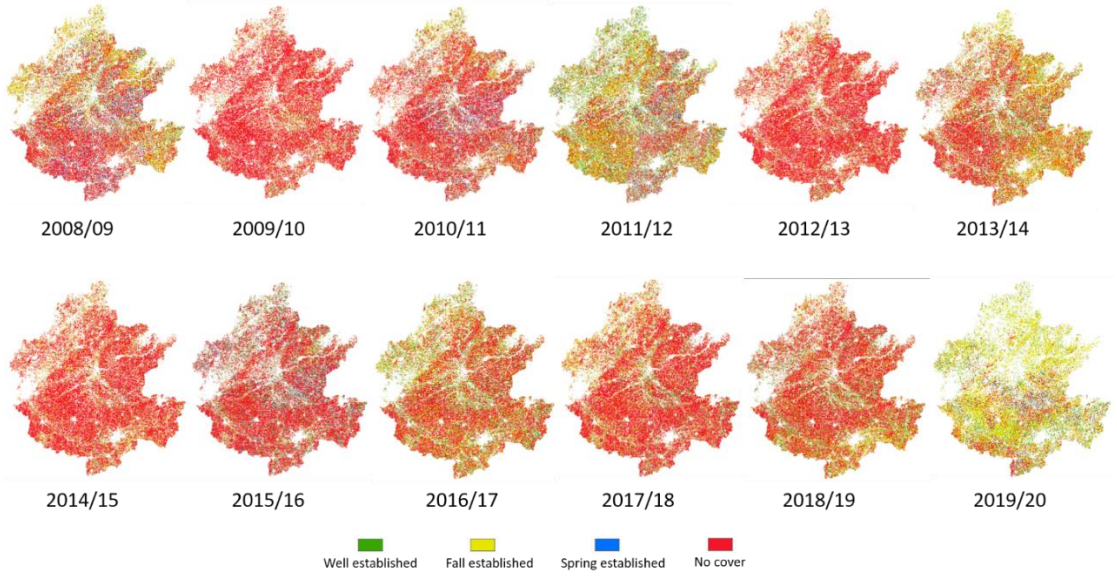

Figure 5: Classification result for all the winter seasons considered in this study for Maumee River watershed. The four classes are represented by different color codes.

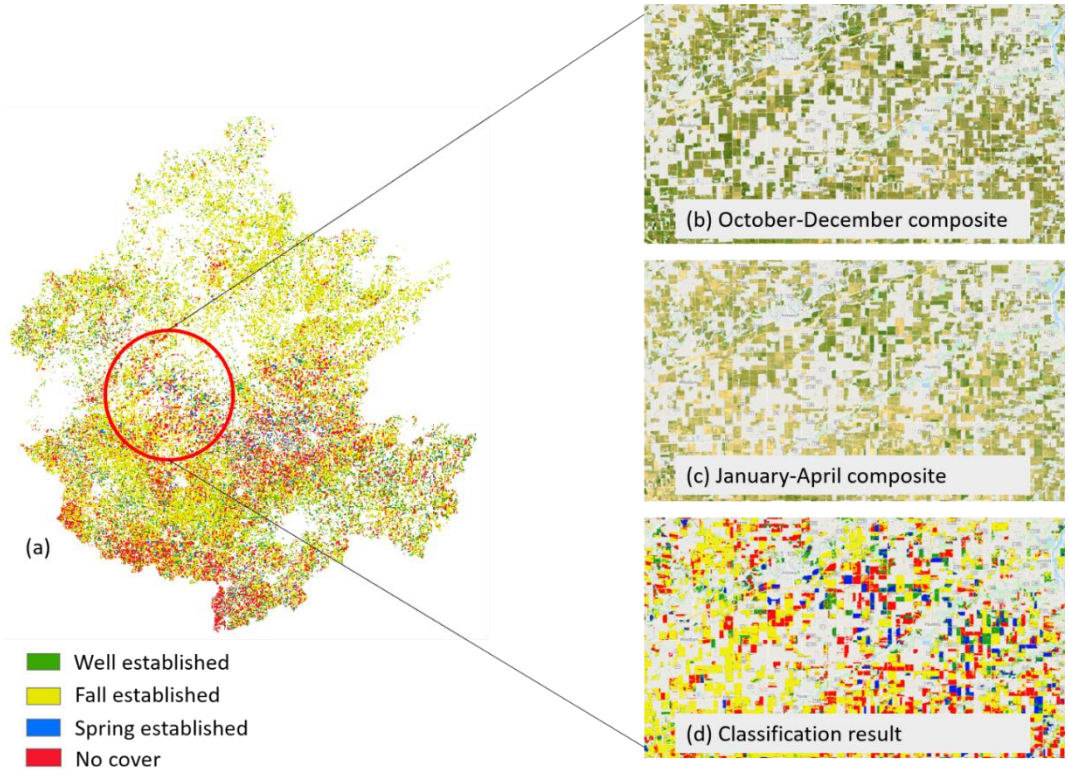

Figure 6: (a) 2019/20 classification result, (b) October-December composite and (c) January-April composite are shown using natural color display of median of Red, Green, and Blue bands. (d) Classification result. (b-d) are zoomed in for an area within (a).

When these areas were evaluated against areas in corn/soybean rotation, it was found that except for 2011/12 and 2019/20 winter seasons, less than 50% of the corn-soybean area in the watershed were in cover crops. While the total corn-soybean area did not change much except for 2019-20 season, we observed variability in the cover crops across the seasons. Although a large percentage of area was covered during fall of 2019/2020 (Figure 6), we found a few percentages of those covers staying on the ground until spring. Similarly, the 2009/10 season had almost 80% of the corn-soybean area without any type of cover and less than 10% for all three cover classes. If we look at the whole time series, cover crop areas (winter hardy, winter kill and spring emergent) seem to have increased from 2008/09 until 2010/11 season. After that, we do not observe any remarkable increase as the larger percentage of winter kill in 2019/20 can be attributed to the decreased corn-soybean area (Figure 7).

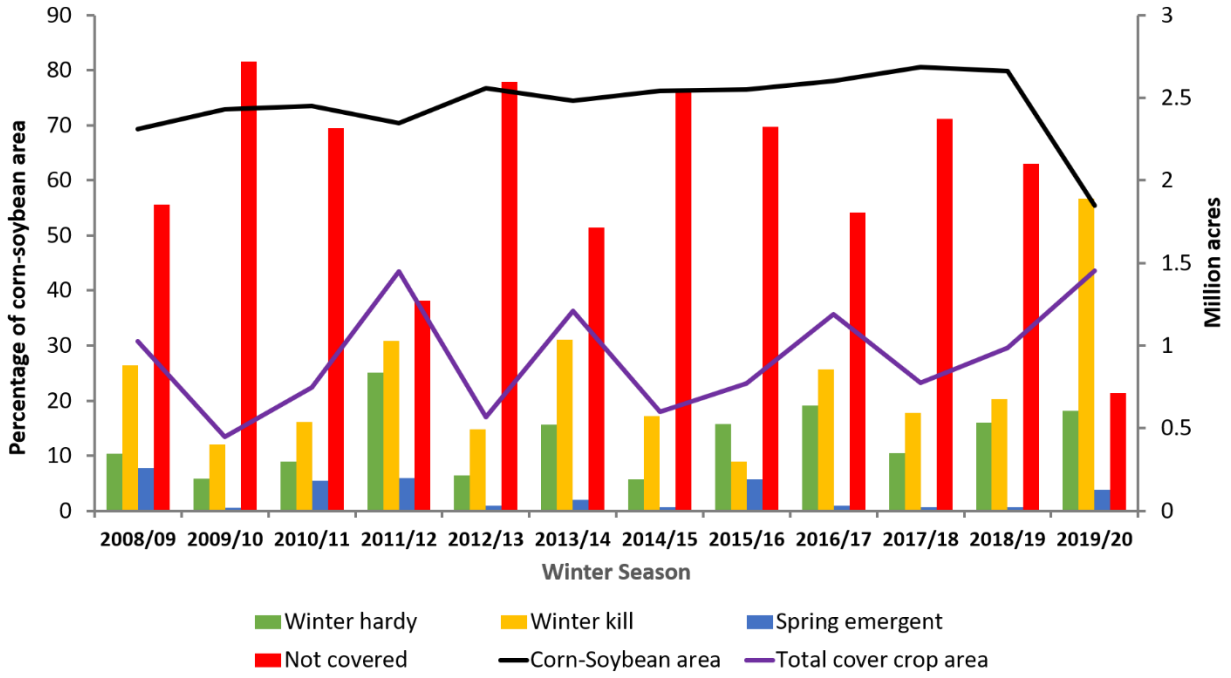

Figure 7: Seasonal variability of winter cover crops between 2008 – 2019. Note: The % area of each class was computed relative to total annual corn-soybean area in given year. The x-axis represents the winter season. The total cover crop area is the sum of three cover crop classes: winter hardy, winter kill, and spring emergent. The secondary y-axis is for total cover crop area and corn-soybean area in terms of million acres.

When we combine the three different types of cover crops (winter hardy, winter kill, and spring emergent, we can observe this uneven trend in cover crop areas over the years. Although the total area has increased by about 40% in 2019/20 season compared to 2008/09 season, it went through number of increase and decrease patterns within space of single season as shown in Figure 7.

3.3 Effects of weather on variation in winter cover

While evaluating winter cover in relation to GDD for fall and spring, GDD was found to be relatively higher for fall of 2011, 2015-2017, and spring of 2010, 2012, 2016, and 2017. In these years, the area of winter hardy class is higher which is also indicated by the strong correlation in Figure 8. Similarly, the spring emergent was higher for 2009, 2011, 2012, and 2016. Regarding the winter kill class, it is correlated well with GDD during fall of 2011, 2013, and 2016. However, it deviates strongly for the 2019 which is also reflected on the weaker correlation (-0.12). Higher amount of GDD throughout the season means more favorable time for full growth of cover crops. This shows that GDD can explain some of the variability in different types of covers during the cover crops seasons.

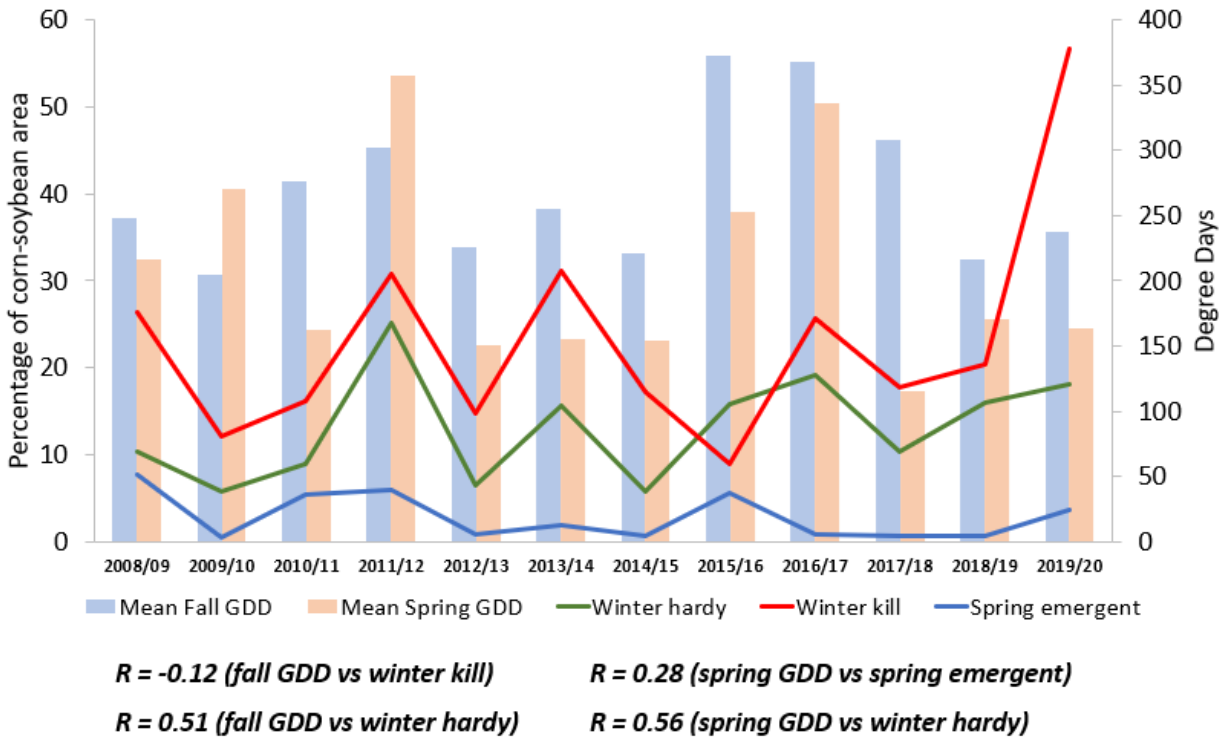

Figure 8: Relationship of cover crops with Growing Degree Days (GDD) and Fall precipitation. Note that the first part in season indicates fall season while the second part indicates spring. For example, if the season is 2008/09, fall season is in 2008 whereas spring in 2009.

The accumulated precipitation was higher for fall of 2011, 2017, and 2018 cover crop seasons. These seasons had relatively larger area of covers (Figure 8). The 2011/12, 2015/16, and 2016/17 seasons are observed to have highest GDD (both fall and spring) as well as accumulated precipitation during fall (Figure 8-11), suggesting that higher accumulative GDD and fall precipitation help promote establishment of cover crops and their growth through the season.

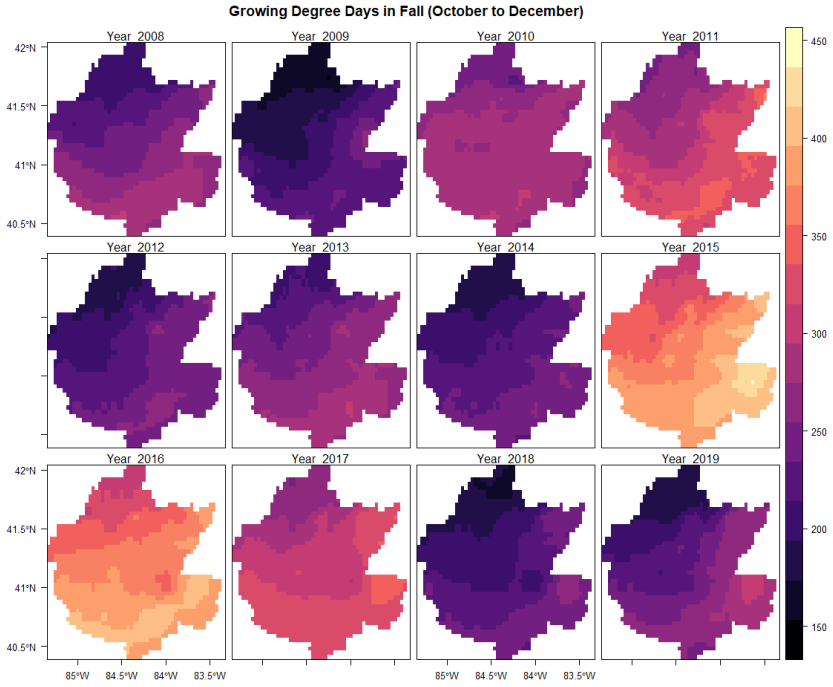

Figure 9: Growing Degree Days during fall calculated for the Maumee River watershed using PRISM daily temperature data at 4 km spatial resolution. The years indicated in this figure correspond to the years for fall seasons.

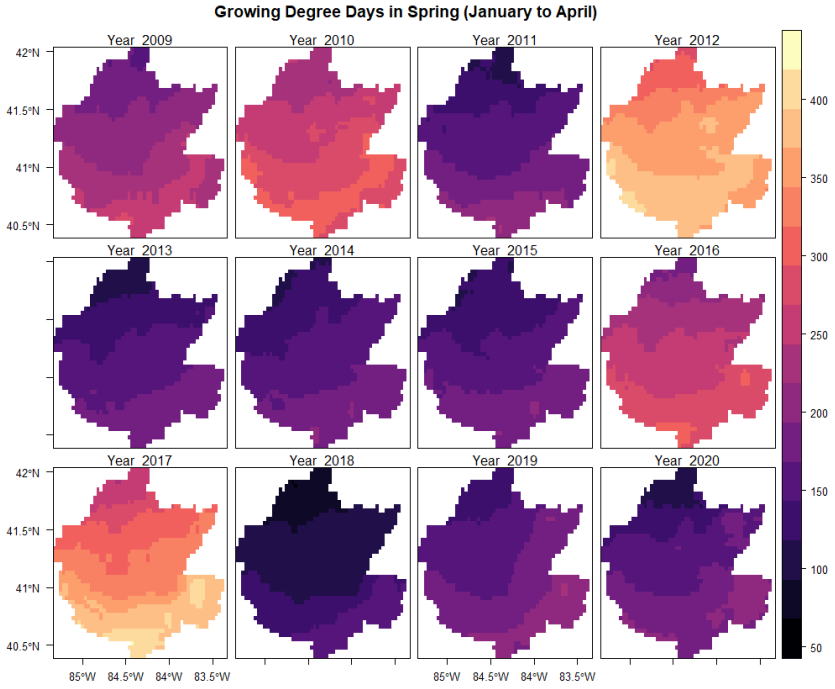

Figure 10: Growing Degree Days calculated for spring. The years indicated here is for the spring months of the following year.

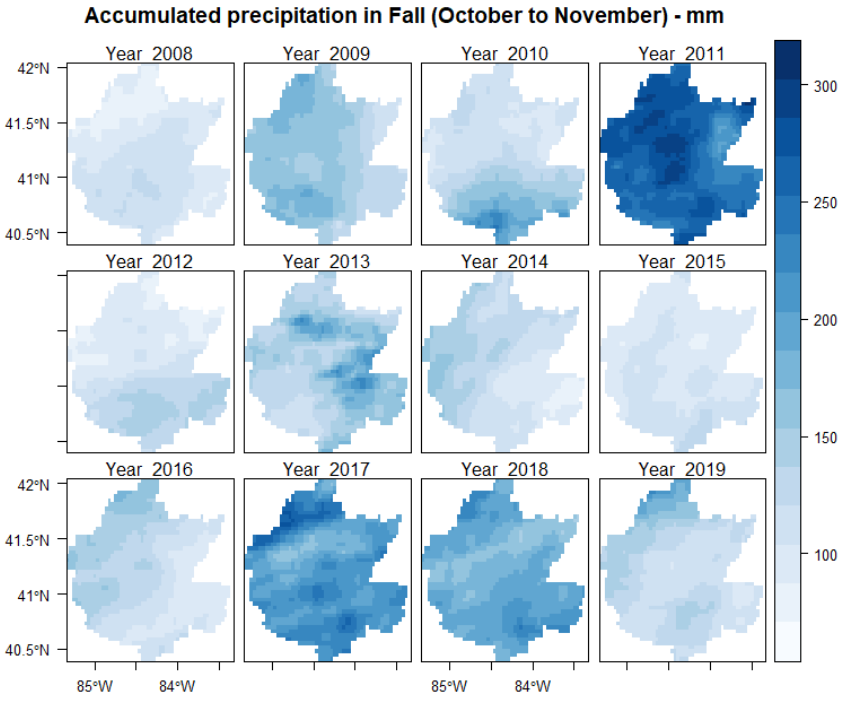

Figure 11: Total precipitation for the fall months of October and November. It is based on PRISM daily precipitation raster data with spatial resolution of 4 km. The years indicated in this figure represent the years of the fall months of October and November.

4. Discussions

In this study, we developed a framework to use publicly available Landsat satellite images to identify four types of winter cover on the corn and soybean rotated fields in the Maumee River watershed. For this, we first prepared the database of fields with cover crops through digitization of tillage transect and survey data. Although these fields were labeled as cover cropped, they were based on a one-time survey, and no additional information on cover crop growth stages during the season were provided. Therefore, the fields were grouped into four categories – winter hardy, winter kill, spring emergent, and no cover, which were derived based on their average greenness i.e., NDVI during fall and spring of the cover cropping seasons. We then extracted spectral information for all the pixels within these fields using satellite image composites, and then trained

a RF classifier. The overall classification accuracy was 75%, and there are few areas that needs to be considered to this number. We believe having this kind of spatial and temporal information on cover cropping could be valuable to policy makers as well as funding agencies to localize the area in need of interventions for supporting adoption of cover cropping practice. Further, it also provides basis for conducting studies on assessing the effectiveness of the practice.

4.1 Training data size

One of the major challenges in performing a pixel level classification is the need to address spatially autocorrelation. If pixels in training and validation dataset are highly correlated, it may then lead to overestimation of classification accuracy as well as too many misclassifications. To address this concern, the pixels from same fields are not included both in training as well as validation data. While this helps in eliminating the most common form of spatial correlation among the pixels, there are still some forms of misclassification on the final estimation. In the study, we used a total of 657 fields as a basis of classification. Although there is no set standard for the training and testing data size suitable for classification problems like this, given the size of landscape used in our study, we expect increase in classification accuracy with additional ground-truth data. Additionally, we did not have ground-truth seasonal cover crop growth information. Although the fields were marked as cover crops, the satellite imagery consistently showed low vegetation during the growing season in some of the fields. While we relied on analyses of NDVI to assess seasonal cover crop growth, ground-truth information would help enhance the accuracy of our cover crop classification model.

In the study, we assumed that all the green areas in the corn and soybean fields during months of October – April are to be in cover crops. However, all the green areas are not necessarily cover crops; they could be either weed or grass or other crops. So, caution needs to be paid while interpreting some of these results.

In the study, misclassification was prominent for the spring emergent class and this can be attributed to fewer training and test dataset. Of 657 fields, we found 24 to be in spring emergent class based on NDVI phenology. Similarly, the average NDVI value greater than or equal to 0.3 was used as a criterion to classify images into four groups. In this process, anything below 0.3 would be classified as no cover crops even if there are some vegetation on the ground for both fall and spring seasons [25]. Additionally, when the fields were grouped into four classes based on the mean seasonal NDVI, there could be areas within the field with NDVI that are either higher or lower than the average Since all the pixels within a field are labeled same and are used for training, this can lead to misclassification if there is high with-in field variability. This is part of the reason why a large proportion of spring emergent pixels were misclassified as no cover and winter hardy classes. By increasing the number of training data in the classification model, the model will be able to separate spectral variability between classes, and thus resulting in higher accuracy.

In the classified cover crop maps, we observe a lot of within-field variation. This is partly driven by the fact that we used pixel-based classification, meaning spectral signature of a given pixel is assessed independent of its surrounding pixels. There were pixels that were completely different from their neighboring pixels, which can result while using composite images from multiple satellite sensors. Although compositing helps to fill in missing data (especially in case of Landsat 7), we observed some forms of artifacts when images have a high amount of scan line errors, which is one of the concerns that are difficult to address when it comes to application of satellite images.

4.2 Variation in winter cover and effects of weather

Of the several factors such as management practices, weather, topography, and soil conditions that can influence cover crop areas, we evaluated the impact of weather, mainly precipitation and GDD, on spatial and temporal variability in the Maumee River watershed.

Similar to prior studies, we found fall precipitation to be correlated with percent cover crop areas. Fall precipitation is considered to be important for cover crop emergence, mainly to those that are aerially seeded, as increase in soil moisture after rainfall helps increase the soil to seed contact required for germination. In a two-year field study, Gaudlip et al (2019) observed differences in cover crop emergence and stand establishment through aerial seeding and related those differences with fall precipitation [16]. Particularly, they observed lower emergence and stand establishment with less fall precipitation in 2017 and higher success in cover crop establishment in very wet fall of 2018 when seeds were aerially applied. However, they found very wet condition unfavorable for cover crops' emergence when seeds were drilled. The study also found fall biomass of cover crops to be correlated well with GDD for both years (R^2 = 0.28 in 2017 and 0.82 in 2018) (Gaudlip et al., 2019).

Cover crop adoption has been reported to be very less in the Maumee watershed compared to other in previous studies. When compared between the two watersheds: Saginaw and Maumee based on several survey reports in 2012, 2014, and 2016 for farmer adoption of conservation practices, only 26.2% of Maumee farmers reported of using cover crops compared to 51% in Saginaw watershed [67]. Although most of the farmers had higher perceptions of risks related to water quality, they believe that they face barriers to cover crop adoption. The study showed that only 26% of the farmers were enrolled in incentive programs including EQIP, CRP, and CSP. This could be one reason we see continuously less area of row crop acres in winter cover in the time series except for 2019/20 season. During 2019/20 season more than 50% of the row crop acres was however observed to be covered in fall. This seems unusual in the time series trend when we look back to previous

years with a sudden spike in the area of cover in fall while the spring cover and fully covered categories consist of only small fraction of area.

The 2019 crop year (from January to August) was one of the wettest in 125 years in the whole contiguous United States including the Midwest [68]. This led to the delay in crop growing season of 2019 by about 3-4 weeks in the Midwest [68]. In Ohio, during the second week of May, only 1-4% of the total acres (corn and soybean) were planted with corn and soybean compared to 47% (corn) and 20% (soybean) for 2014-2018 on average and 50%(corn) and 28%(soybean) previous year [69]. The Ohio NRCS even announced a disaster recovery funding to the farmers to plant cover crops on their flooded cropland where they were not able plant their regular cash crops [70]. This type of program was introduced around the whole Midwest. It means that most of the row crop acres had cover crop from the previous growing season. This could be the reason why our model detected a large fraction of corn-soybean area in the Maumee River watershed as being classified as fall established.

Although the ground truth data were representative of the cover crops in the fields, our model however does not have ability to differentiate between weed and cover crops. If there is a presence of weed, having spectrally similar pattern as the healthy growing crops, the model just classifies that as cover crops. This could be potentially other reason that we observe larger proportion of fall established covers than the fully established and spring established covers. The probability of cover crops/cover crop fields getting weed biomass increases during fall if the length of growing season is longer than the normal [45].

The longer growing season means higher growing degree days (GDD) which is one of the important variables/predictors explaining the weed biomass in the fall. Baraibar et al. (2018) reported that there exists a correlation between cover crop and weed biomass in the fall. While during spring the relation is just opposite as the higher amount of cover crop biomass suppresses the growth of weed.

5. Conclusions

In this study, we implemented satellite remote sensing and machine learning approach to detect spatial and temporal trends of winter covers in the Maumee River watersheds in northwestern Ohio and understand their relationship with weather factor. A RF based machine learning model was trained by integrating ground-truth field data with the seasonal satellite image composites developed utilizing Landsat 5,7 and 8 captured scenes. The study focused mainly on corn and soybean fields, and the information about corn and soybean fields on an annual scale was obtained from USDA cropland data layers. The temporal variability of cover crops was analyzed with fall precipitation and GDD to understand the role of weather in establishment and growth of cover crops through the season. The model once trained was then used to classify the fields into four categories – (1) winter kill, (2) winter hardy, (3) spring emergent, and (4) no cover. Our results show that for most part of the study period, more than 40% of the corn-soybean area in the watershed was not covered with winter vegetation. Winter cover crop area in the Maumee River watershed has increased by about 40% in 2019/20 season compared to 2008/09 season. Similarly, the cover crops are found to perform well when the weather is favorable during early establishment as well as through the whole season. This study shows that cover cropping practice can be monitored at a landscape scale utilizing publicly available images from earth observing satellites. Understanding of cover cropping practices at a landscape scale is significant to developing critical public policies for increasing the adoption and improving overall sustainability of agricultural production system.

6. References

1. Dabney, S. M., Delgado, J. A. & Reeves, D. W. Using winter cover crops to improve soil and water quality. *Commun. Soil Sci. Plant Anal.* **32**, 1221–1250 (2001).
2. Sharpley, A. N. *et al.* Best Management Practices To Minimize Agricultural Phosphorus Impacts on Water Quality. *United States Dep. Agric.* **ARS-163**, (2006).
3. Villamil, M. B., Bollero, G. A., Darmody, R. G., Simmons, F. W. & Bullock, D. G. No-Till Corn/Soybean Systems Including Winter Cover Crops. *Soil Sci. Soc. Am. J.* **70**, 1936–1944 (2006).
4. Strock, J. S., Porter, P. M. & Russelle, M. P. Cover Cropping to Reduce Nitrate Loss through Subsurface Drainage in the Northern U.S. Corn Belt. *J. Environ. Qual.* **33**, 1010 (2004).
5. Muenich, R. L., Kalcic, M. & Scavia, D. Evaluating the Impact of Legacy P and Agricultural Conservation Practices on Nutrient Loads from the Maumee River Watershed. *Environ. Sci. Technol.* **50**, 8146–8154 (2016).
6. Parr, M., Grossman, J. M., Reberg-Horton, S. C., Brinton, C. & Crozier, C. Nitrogen Delivery from Legume Cover Crops in No-Till Organic Corn Production. *Agron. J.* **103**, 1578–1590 (2011).
7. Behnke, G. D. & Villamil, M. B. Cover crop rotations affect greenhouse gas emissions and crop production in Illinois, USA. *F. Crop. Res.* **241**, 107580 (2019).
8. Brennan, E. B. & Smith, R. F. Winter Cover Crop Growth and Weed Suppression on the Central Coast of California Author (s): Eric B . Brennan and Richard F . Smith Published by : Cambridge University Press on behalf of the Weed Science Society of America Stable URL : https://www.jstor. *Weed Technol.* **19**, 1017–1024 (2005).
9. Wilcoxen, C. A., Walk, J. W. & Ward, M. P. Use of cover crop fields by migratory and resident birds. *Agric. Ecosyst. Environ.* **252**, 42–50 (2018).
10. Roesch-Mcnally, G. E. *et al.* The trouble with cover crops: Farmers' experiences with overcoming barriers to adoption. *Renew. Agric. Food Syst.* **33**, 322–333 (2018).
11. Gould, W. Remote sensing of vegetation, plant species richness, and regional biodiversity hotspots. *Ecol. Appl.* **10**, 1861–1870 (2000).
12. Benedetti, R., Rossini, P. & Taddei, R. Vegetation classification in the Middle Mediterranean area by satellite data. *Int. J. Remote Sens.* **15**, 583–596 (1994).
13. Wardlow, B. D. & Egbert, S. L. Large-area crop mapping using time-series MODIS 250 m NDVI data: An assessment for the U.S. Central Great Plains. *Remote Sens. Environ.* **112**, 1096–1116 (2008).
14. Tian, H. *et al.* Mapping Winter Crops in China with Multi-Source Satellite Imagery and Phenology-Based Algorithm. *Remote Sens.* **11**, (2019).
15. Savage, S. L. *et al.* Shifts in Forest Structure in Northwest Montana from 1972 to 2015 Using the Landsat Archive from Multispectral Scanner to Operational Land Imager. *Forests* **9**, (2018).
16. Gaudlip, C., Sedghi, N., Fox, R., Sherman, L. & Weil, R. Effective Cover Cropping in Extremes of Weather. (2019).
17. Frazier, R. J., Coops, N. C., Wulder, M. A. & Kennedy, R. Characterization of aboveground biomass in an unmanaged boreal forest using Landsat temporal segmentation metrics. *ISPRS J. Photogramm. Remote Sens.* **92**, 137–146 (2014).
18. Boryan, C., Yang, Z., Mueller, R. & Craig, M. Monitoring US agriculture: the US Department of Agriculture, National Agricultural Statistics Service, Cropland Data Layer Program. *Geocarto Int.* **26**, 341–358 (2011).
19. Vogelmann, J. E. *et al.* Completion of the 1990s National Land Cover Data set for the conterminous United States from Landsat Thematic Mapper data and ancillary data sources. *Photogramm. Eng. Remote Sensing* **67**, 650–662 (2001).
20. Wardlow, B. D., Egbert, S. L. & Kastens, J. H. Analysis of time-series MODIS 250 m vegetation index data for crop classification in the U.S. Central Great Plains. *Remote Sens. Environ.* **108**, 290–310 (2007).
21. Rundquist, S. & Carlson, S. Mapping Cover Crops on Corn and Soybeans in Illinois , Indiana and Iowa, 2015-2016. *Environ. Work. Group. Washington, D.C* 2015–2016 (2017).
22. Hagen, S. C. *et al.* Mapping conservation management practices and outcomes in the corn belt using the operational tillage information system (Optis) and the denitrification–decomposition (DNDC) model. *Land* **9**, 1–23 (2020).
23. Tao, Y. & You, F. Prediction of Cover Crop Adoption through Machine Learning Models using Satellite-derived Data. *IFAC-PapersOnLine* **52**, 137–142 (2019).
24. Seifert, C. A., Azzari, G. & Lobell, D. B. Satellite detection of cover crops and their effects on crop yield in the Midwestern United States. *Environ. Res. Lett.* **14**, (2018).
25. Thieme, A. *et al.* Using NASA Earth observations and Google Earth Engine to map winter cover crop conservation performance in the Chesapeake Bay watershed. *Remote Sens. Environ.* **248**, 111943 (2020).
26. Hively, W. D., Duiker, S., McCarty, G. & Prabhakara, K. Remote sensing to monitor cover crop adoption in southeastern Pennsylvania. *J. Soil Water Conserv.* **70**, 340–352 (2015).
27. Azzari, G. & Lobell, D. B. Landsat-based classification in the cloud: An opportunity for a paradigm shift in land cover monitoring. *Remote Sens. Environ.* **202**, 64–74 (2017).
28. Gorelick, N. *et al.* Google Earth Engine: Planetary-scale geospatial analysis for everyone. *Remote Sens. Environ.*

202, 18–27 (2017).
29. Xiong, J. *et al.* Automated cropland mapping of continental Africa using Google Earth Engine cloud computing. *ISPRS J. Photogramm. Remote Sens.* **126**, 225–244 (2017).
30. Xie, Y., Lark, T. J., Brown, J. F. & Gibbs, H. K. Mapping irrigated cropland extent across the conterminous United States at 30 m resolution using a semi-automatic training approach on Google Earth Engine. *ISPRS J. Photogramm. Remote Sens.* **155**, 136–149 (2019).
31. Oliphant, A. J. *et al.* Mapping cropland extent of Southeast and Northeast Asia using multi-year time-series Landsat 30-m data using a random forest classifier on the Google Earth Engine Cloud. *Int. J. Appl. Earth Obs. Geoinf.* **81**, 110–124 (2019).
32. Campos-Taberner, M. *et al.* Global Estimation of Biophysical Variables from Google Earth Engine Platform. *Remote Sens.* **10**, (2018).
33. Traganos, D. *et al.* Towards Global-Scale Seagrass Mapping and Monitoring Using Sentinel-2 on Google Earth Engine: The Case Study of the Aegean and Ionian Seas. *Remote Sens.* **10**, (2018).
34. Martin, J. *et al.* Evaluating management options to reduce Lake Erie algal blooms using an ensemble of watershed models. *J. Environ. Manage.* **280**, (2020).
35. *Ohio Lake Erie Phosphorus Task Force Final Report*. http://epa.ohio.gov/portals/35/lakeerie/ptaskforce/task_force_final_report_april_2010.pdf (2013).
36. Burnett, E. A., Howard, G., Irwin, E., Wilson, R. S. & Martin, J. *F Armers , P Hosphorus and W Ater Q Uality : P Art Ii a Descriptive Report of Beliefs , Attitudes and Best*. (2015) doi:10.13140/RG.2.1.3317.0805.
37. Masek, J. G. *et al.* A Landsat surface reflectance dataset for North America, 1990-2000. *IEEE Geosci. Remote Sens. Lett.* **3**, 68–72 (2006).
38. Vermote, E., Justice, C., Claverie, M. & Franch, B. Preliminary analysis of the performance of the Landsat 8/OLI land surface reflectance product. *Remote Sens. Environ.* **185**, 46–56 (2016).
39. Foga, S. *et al.* Cloud detection algorithm comparison and validation for operational Landsat data products. *Remote Sens. Environ.* **194**, 379–390 (2017).
40. Roy, D. P. *et al.* Characterization of Landsat-7 to Landsat-8 reflective wavelength and normalized difference vegetation index continuity. *Remote Sens. Environ.* **185**, 57–70 (2016).
41. Vogeler, J. C., Braaten, J. D., Slesak, R. A. & Falkowski, M. J. Extracting the full value of the Landsat archive: Inter-sensor harmonization for the mapping of Minnesota forest canopy cover (1973–2015). *Remote Sens. Environ.* **209**, 363–374 (2018).
42. Azzari, G. *et al.* Satellite mapping of tillage practices in the North Central US region from 2005 to 2016. *Remote Sens. Environ.* **221**, 417–429 (2019).
43. Carrasco, L., O'Neil, A. W., Morton, R. D. & Rowland, C. S. Evaluating Combinations of Temporally Aggregated Sentinel-1, Sentinel-2 and Landsat 8 for Land Cover Mapping with Google Earth Engine. *Remote Sens.* **11**, (2019).
44. Teluguntla, P. *et al.* A 30-m landsat-derived cropland extent product of Australia and China using random forest machine learning algorithm on Google Earth Engine cloud computing platform. *ISPRS J. Photogramm. Remote Sens.* **144**, 325–340 (2018).
45. Baraibar, B. *et al.* Growing degree days and cover crop type explain weed biomass in winter cover crops. *Agron. Sustain. Dev.* **38**, (2018).
46. Oregon State University. PRISM Climate Group. https://prism.oregonstate.edu/explorer/.
47. Ghazaryan, G. *et al.* A rule-based approach for crop identification using multi-temporal and multi-sensor phenological metrics. *Eur. J. Remote Sens.* **51**, 511–524 (2018).
48. Jakubauskas, M. E., Legates, D. R. & Kastens, J. H. Harmonic analysis of time-series AVHRR NDVI data. *Photogramm. Eng. Remote Sensing* **67**, 461–470 (2001).
49. Jakubauskas, M. E., Legates, D. R. & Kastens, J. H. Crop identification using harmonic analysis of time-series AVHRR NDVI data. *Comput. Electron. Agric.* **37**, 127–139 (2002).
50. USDA. CropScape - Cropland Data Layer. https://nassgeodata.gmu.edu/CropScape/.
51. Moreno-Martínez, Á. *et al.* Multispectral high resolution sensor fusion for smoothing and gap-filling in the cloud. *Remote Sens. Environ.* **247**, 111901 (2020).
52. Townshend, J. R. G. & Justice, C. O. Analysis of the dynamics of African vegetation using the normalized difference vegetation index. *Int. J. Remote Sens.* **7**, 1435–1445 (1986).
53. Bellón, B., Bégué, A., Lo Seen, D., De Almeida, C. A. & Simões, M. A Remote Sensing Approach for Regional-Scale Mapping of Agricultural Land-Use Systems Based on NDVI Time Series. *Remote Sens.* **9**, (2017).
54. Tucker, C. J. Red and photographic infrared linear combinations for monitoring vegetation. *Remote Sens. Environ.* **8**, 127–150 (1979).
55. Jordan, C. F. Derivation of Leaf-Area Index from Quality of Light on the Forest Floor. *Ecology* **50**, 663–666 (1969).
56. Haas, J. & Ban, Y. Urban growth and environmental impacts in Jing-Jin-Ji, the Yangtze, River Delta and the Pearl River Delta. *Int. J. Appl. Earth Obs. Geoinf.* **30**, 42–55 (2014).

57. Belgiu, M. & Drăguţ, L. Comparing supervised and unsupervised multiresolution segmentation approaches for extracting buildings from very high resolution imagery. *ISPRS J. Photogramm. Remote Sens.* **96**, 67–75 (2014).
58. Karlson, M. *et al.* Mapping Tree Canopy Cover and Aboveground Biomass in Sudano-Sahelian Woodlands Using Landsat 8 and Random Forest. *Remote Sens.* **7**, 10017–10041 (2015).
59. Nitze, I., Schulthess, U. & Asche, H. Comparison of machine learning algorithms random forest, artificial neuronal network and support vector machine to maximum likelihood for supervised crop type classification. *Proc. 4th Conf. Geogr. Object-Based Image Anal. – GEOBIA 2012* 35–40 (2012).
60. Ok, A. O., Akar, O. & Gungor, O. Evaluation of random forest method for agricultural crop classification. *Eur. J. Remote Sens.* **45**, 421–432 (2012).
61. Rodriguez-Galiano, V. F., Chica-Olmo, M., Abarca-Hernandez, F., Atkinson, P. M. & Jeganathan, C. Random Forest classification of Mediterranean land cover using multi-seasonal imagery and multi-seasonal texture. *Remote Sens. Environ.* **121**, 93–107 (2012).
62. Pelletier, C., Valero, S., Inglada, J., Champion, N. & Dedieu, G. Assessing the robustness of Random Forests to map land cover with high resolution satellite image time series over large areas. *Remote Sens. Environ.* **187**, 156–168 (2016).
63. Belgiu, M. & Drăgu, L. Random forest in remote sensing: A review of applications and future directions. *ISPRS J. Photogramm. Remote Sens.* **114**, 24–31 (2016).
64. Breiman, L. Random Forests. *Mach. Learn.* **45**, 5–32 (2001).
65. Rodriguez-Galiano, V. F., Ghimire, B., Rogan, J., Chica-Olmo, M. & Rigol-Sanchez, J. P. An assessment of the effectiveness of a random forest classifier for land-cover classification. *ISPRS J. Photogramm. Remote Sens.* **67**, 93–104 (2012).
66. Gislason, P. O., Benediktsson, J. A. & Sveinsson, J. R. Random forests for land cover classification. *Pattern Recognit. Lett.* **27**, 294–300 (2006).
67. Tellez, C. & Wilson, R. S. *Researching the effectiveness of agricultural programs: Evaluating survey data in the Maumee and Saginaw Watersheds*. (2018).
68. Yin, Y. *et al.* Cropland Carbon Uptake Delayed and Reduced by 2019 Midwest Floods. *AGU Adv.* **1**, 1–15 (2020).
69. USDA. Economics, Statistics and Market Information System. https://usda.library.cornell.edu/concern/publications/8336h188j?locale=en#release-items (2019).
70. USDA NRCS. Ohio NRCS Announces Disaster Recovery Funding to Plant Cover Crops on Flooded Cropland Acreage. https://www.nrcs.usda.gov/wps/portal/nrcs/oh/newsroom/releases/52bc20f8-c480-4908-848b-1546ca68a182/ (2019).